JAMES C. KECK (*)

Mechanism of air pollutant formation in internal combustion engines (**).

Abstract — *This paper summarizes the research being conducted in the Mechanical Engineering Department at the Massachusetts Institute of Technology on the mechanism of air pollutant formation in internal combustion engines. Four basic problems are discussed:* 1) *the aerodynamics of the hydrocarbon rich boundary layers,* 2) *the thermodynamics of internal combustion,* 3) *the mechanism of* NO *formation and* 4) *the effect of threebody reactions on the formation of* CO. *Some practical applications of the research to the reduction of air pollution are also suggested.*

Internal combustion engines are the largest single source of air pollution in urban areas of the United States. They produce 90% of the carbon monoxide CO, 50% of the oxides of nitrogen NO_x, and 70% of the unburned hydrocarbons. In the presence of sunlight these pollutants further react with air to produce the extremely objectionable photochemical smog typical of that found in the Los Angeles basin and I believe also here in the Piedmonte region.

Since air pollution was recognized as a critical problem approximately ten years ago many possible solutions have been proposed. Some of these involve replacing internal combustion engines with other power plants such as electric motors or steam engines. Other involve improved mass transportation systems to reduce the number of cars on the road. Last but not least, there is the possibility of modifying the internal combustion engine to decrease the pollution it produces. This is the approach I shall consider in the present paper.

Today there are dozens of technically feasible methods of reducing air pollution from internal combustion engines to acceptable levels. All of them, however, involve some compromise in either performance, realibility, or cost. The problem therefore is not so much to find *a* solution but to find the *optimum combination* of solutions. To do this with any degree of confidence, it is necessary to have a basic understanding of the processes by which pollutants are formed in internal combustion engines.

(*) Ford Professor of Engineering.

(**) This work was supported in part by grants from the M. I. T. Sloan Basic Research Fund, and the M. I. T. Urban System Laboratories.

Obviously a high level of confidence is particularly important in this case because of the tremendous capital investment required to make even minor modifications in the millions of engines produced annually.

To assist with the problem, the Thermodynamics and Fluid Mechanics groups in the Mechanical Engineering Department of the Massachusetts Institute of Technology have been studying the fundamental processes responsible for pollutant formation in internal combustion engines. Four basic problems are being investigated: 1) the aerodynamics of the hydrocarbon rich boundary layers on the cylinder walls; 2) the thermodynamics of internal combustion; 3) the mechanism of NO formation and «freezing» in the gas phase; and 4) the effect of three-body reactions on the «freezing» of CO.

Aerodynamics of Boundary Layers.

It has been established in experiments carried out at the General Motors Research Laboratories [1] that the major sources of unburned hydrocarbons in the exhaust of an internal combustion engine are the

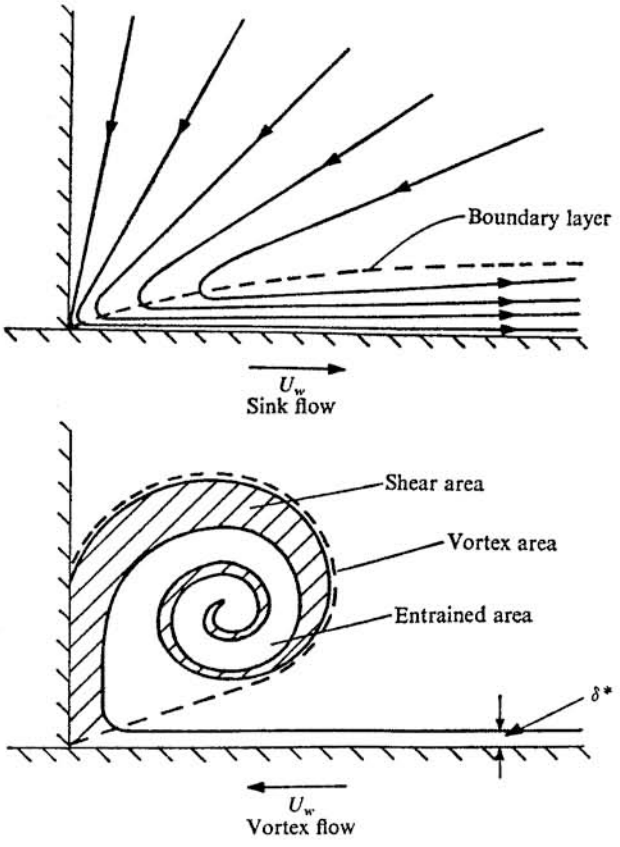

Fig. 1.

Types of boundary flow observed in water analog for retreating (sink flow) and advancing (vortex flow) pistons.

cool boundary layers on the cylinder walls. The question of how these boundary layers are ejected from the cylinder, however, has not yet been answered. Three separate layers whose aerodynamic behavior is expected to be distinctly different must be considered: one on the cylinder head, the second on the piston face, and the third on the cylinder side wall.

In our initial investigations of this problem we have been studying the manner in which the advancing piston scraps up the side wall boundary

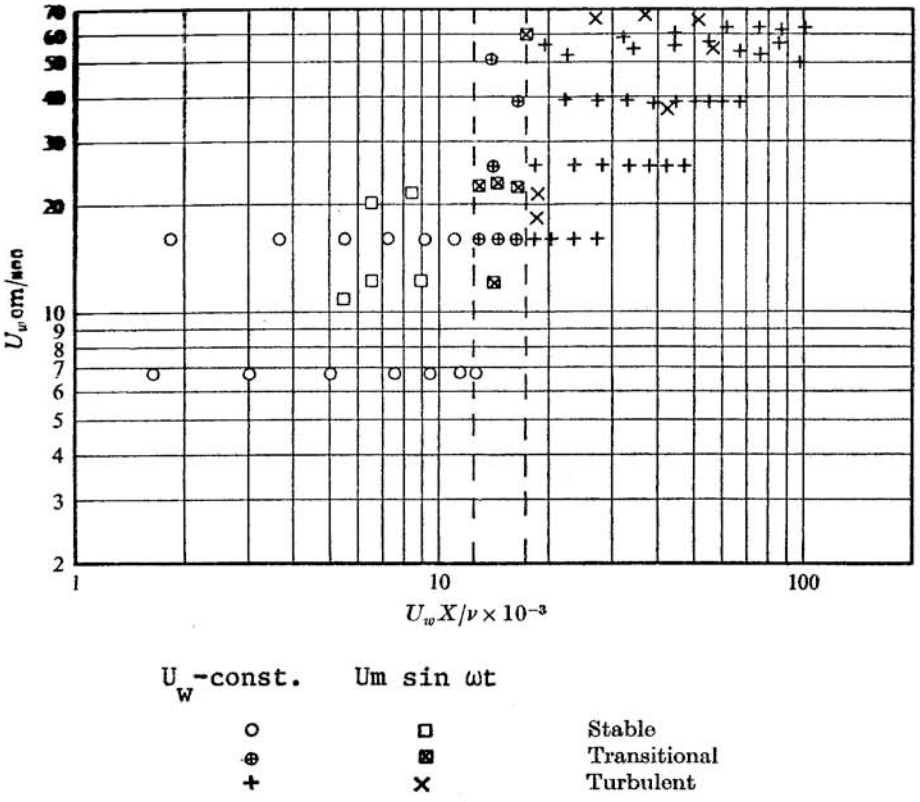

Fig. 2.

Character of vortex flow as a function of piston velocity and Reynold's number based on stroke.

layer during the exhaust stroke [2]. A water analog of the cylinder of an internal combustion was constructed in which the appropriate Reynold's numbers could be reproduced and the behavior of the boundary layer studied for both advancing and retreating piston. The flow patterns were visualized using both dyes and illuminated fish scales. Unfortunately the original photographs are difficult to reproduce but examples of the types of motion observed are illustrated by the drawings in figure 1. In the case of a retreating piston the boundary layer drags fluid out of the corner between the piston face and the wall resulting in the type of « sink

flow » illustrated in the upper part of the figure. For an advancing piston, which is the case occurring during the exhaust stroke, the piston « roles up » the boundary layer into a spiral vortex having a cross-sectional area very nearly twice the cross-sectional area of the boundary layer swept up. Initially the vortex is laminar as shown in the lower part of fig. 1, however, as the length of the stroke increases the vortex goes through a transition and becomes turbulent.

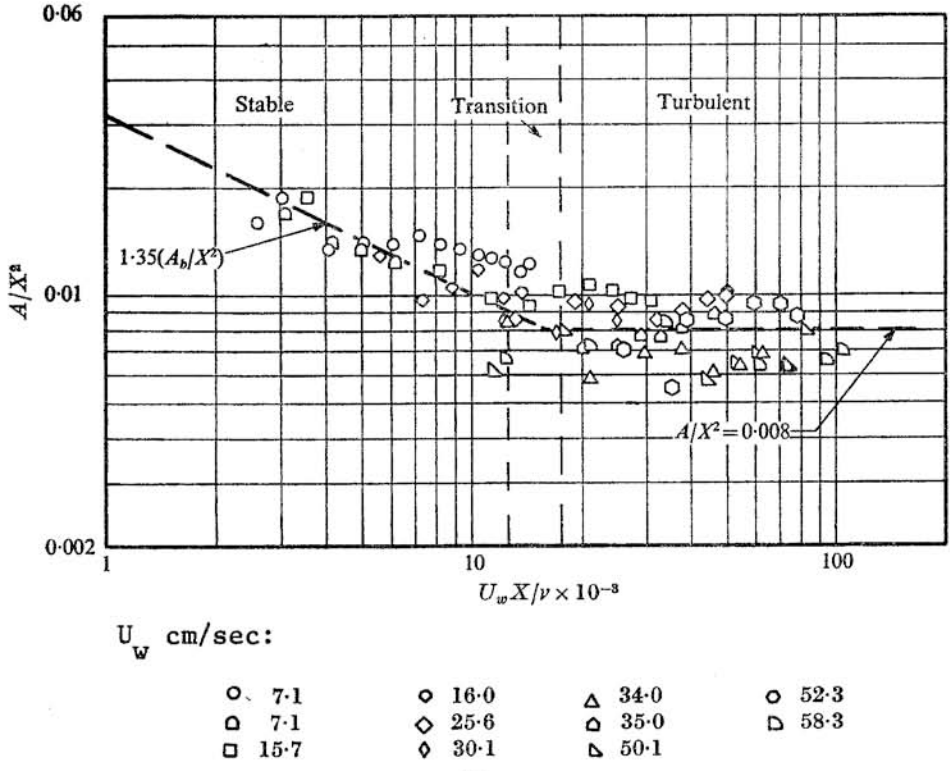

Fig. 3.

Vortex area divided by the stroke length squared as a function of Reynold's number.

The character of the flow for various piston velocities is shown as a function of the Reynold's number based on the length of the stroke X in fig. 2. Most of the data shown are for constant piston velocity but a few runs for a sinusoidally varying velocity are also shown. It can be seen that transition occurs at a Reynold's number of approximately 15000 which is typical of that at the end of the stroke in an internal combustion engine.

Figure 3 shows the cross-sectional area A of the vortex divided by the square of the stroke X^2 as a function of Reynold's number. In the laminar regime where the boundary layer thickness grows as $X^{1/2}$, the vortex area grows as $X^{3/2}$. In the turbulent regime where the boundary layer

grows as X, the vortex area grows as X^2. This is precisely what would be expected from a simple « role up » of the boundary layer.

These results imply that in an internal combustion engine the diameter of the « role up » boundary layer at the end of the stroke will be close to the clearance height. Thus we might expect a large fraction of the unburned hydrocarbons to be ejected at the end of the exhaust stroke. This effect has actually been observed in the General Motors experiments [1] and in experiments currently in progress at M.I.T. We may anticipate from these observations that cylinder head and piston geometry, exhaust valve location, and particularly clearance height at T.D.C. will have an important effect on the emission of unburned hydrocarbons.

Thermodynamic Model of Internal Combustion.

It is well known that in an internal combustion engine the major energy producing reactions are very close to equilibrium and that the trace concentration of pollutants formed have a negligible effect on the overall thermodynamic state of the burned gas. Thus, we may first determine state of the gases within the cylinder using equilibrium thermodynamics and then treat the process of pollutant formation as a perturbation later.

To do this we have developed a simple analytic model [3] of internal combustion which permits one to calculate the thermodynamic state of the gases from a knowledge of the pressure and volume of the system as a function of time. The model asumes that 1) the original charge is homogeneus, 2) the pressure at any time is independent of position, 3) the volume occupied by the nonequilibrium chemical reaction zone is negligible, 4) the burned gas is at full thermodynamic equilibrium, 5) the unburned gas is « frozen » at its original composition and undergoes adiabatic compression, and 6) both burned and unburned gases have constant local specific heats. In most practical engines all these assumptions are well justified. Under these conditions the mass fraction of the burned gas, X, can be calculated from the laws for conservation of mass and energy and the equation of state for the burned and unburned gases. The result is

$$(1) \qquad MX = \frac{pV - p_0V_0 + (\gamma_b - 1)(W + Q) + (\gamma_b - \gamma_u)Mc_{vu}(T_u - T_0)}{(\gamma_b - 1)(h_{fu} - h_{fb}) + (\gamma_b - \gamma_u)c_{vu}T_u}$$

where M is the total mass of gas in the cylinder, p is the pressure, V is the volume, T is the temperature, W is the work done, Q is the heat loss,

c_v is the local specific heat, h_f is the corresponding specific enthalpy of formation, $\gamma = c_p/c_v$ is the specific heat ratio and the subscripts o, u, and b refer to initial conditions, unburned gas, and burned gas respectively.

Typical curves showing the measured pressure and calculated mass fraction burned as a function of crank angle are shown in fig. 4. Combu-

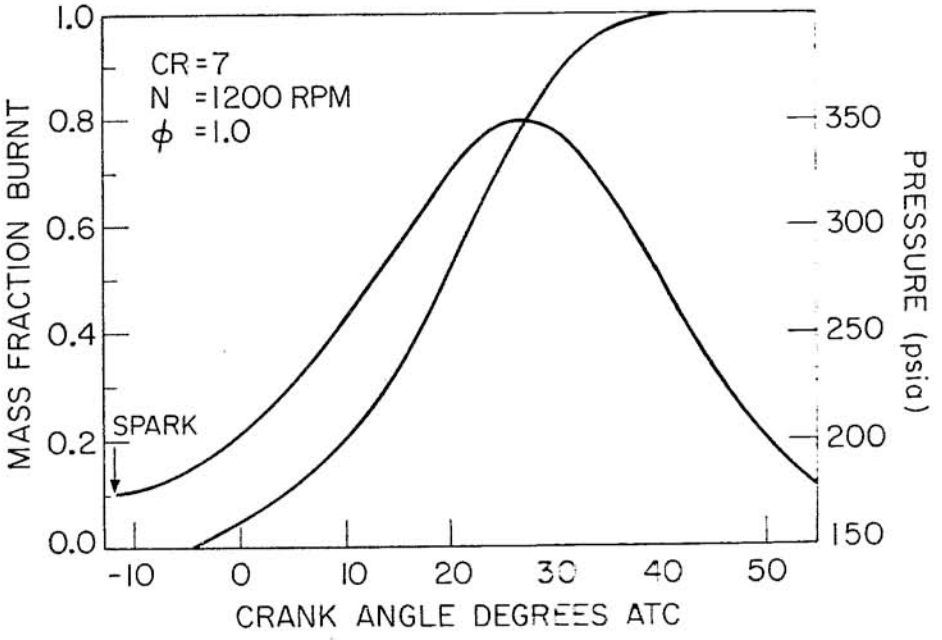

Fig. 4.

Measured pressure and corresponding calculated mass fraction of burned gas as a function of crank angle.

stion is complete and takes about 40 crank angle degrees. Note that as a consequence of the assumption of constant local specific heats, these results are independent of the temperature distribution in the burned gas.

To determine the temperature distribution in the burned gas it is necessary to make an assumption about that state of mixing in these gases. In most previous treatments of this problem [1] it has been assumed that the temperature of the burned gas was uniform corresponding to complete mixing. This gives

$$R_b T_b = R_u T_u + (pV - M R_u T_u) Mx \tag{2}$$

where R is the gas constant. We do not believe that the assumption of complete mixing is a good one, however, because it is incompatible with

both the observations of a relatively thin turbulent flame front and substantial temperature gradients in the burned gas. A much more realistic approximation is to assume that there is no mixing at all and that each element of gas which burns is adiabatically compressed from its state just behind the flame front to its final state. Under these conditions the temperature of an element of gas is given by

$$T_b(X', X) = T_b(X')[p(X)/p(X')]^{(\gamma_b - 1)/\gamma_b} \tag{3}$$

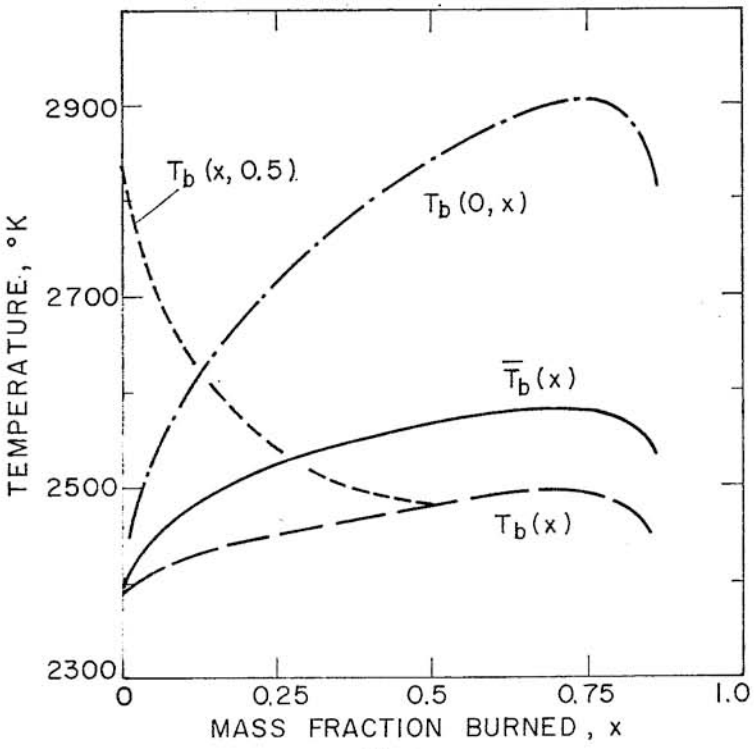

Fig. 5.

Temperature distributions in the burned gas as a function of mass fraction: $T_b(o, X)$ is the temperature of the element which burned first, $T_b(X)$ is the temperature immediately behind the reaction zone, $\overline{T}_b(X)$ is the mean temperature, and $T_b(X, .5)$ is the temperature distribution at a time when combustion is 50% complete.

where $T_b(X', X)$ is the temperature the element which burned at a pressure $p(X')$ when the pressure is $p(X)$, and

$$T_b(X') = [h_{fu} - h_{fb} + c_{pu} T_u(X')]/c_{pu} \tag{4}$$

is the temperature resulting from isenthalpic combustion of the gas at the pressure $p(X')$.

Some typical temperature distributions for the unmixed case are shown in fig. 5 as a function of mass fraction burned. It can be seen that

a substantial temperature gradient exist in the burned gas and that the peak temperature $T_b(O, X)$ of the gas that burned first is approximately 400° K higher than that $T_b(X)$ of the gas immediately behind the flame front. Due to the strong temperature dependence of chemical equilibrium constants and reaction rates, such temperature differences are very important in connection with pollutant formation and can produce order of magnitude variations in concentration levels in the burned gas.

Model of NO Formation.

NO may be formed in internal combustion engines either in the non-equilibrium reaction zone or in the hot burned gases behind the flame front. In our initial investigations, we have concentrated on formation in the burned gas and have developed a model [3] of the process which, for equivalence ratios less than 1.2, agrees well with experimental observations. For richer mixtures, the model underestimates the amount of NO produced which may be an indication that formation in the reaction zone is important in this case.

The model includes consideration of the 12 most abundant species found in an equilibrium mixture of the combustion products of air and C_8H_{18}. These are shown in table 1 along with an indication of their appro-

TABLE I.

Species included in model of NO formation and approximate concentrations at 2500 °K.

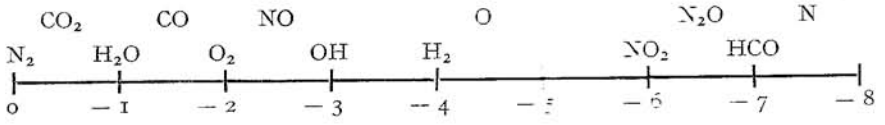

ximate relative concentration at 2500° K. The thermodynamic state of the gas is determined from the model described in the preceding section and the major energy producing reactions involving the C—O—H system are taken to be in equilibrium. The process of NO formation is assumed to be controlled by the 6 reactions shown in table 2 where the exothermicities are given in kcal/mole and the exothermic rate constants [5] are given in cm^3/sec. These equations may be combined to obtain 3 first order non-linear differential equations for the concentrations of N, NO, and N_2O. Although numerical integration of the full set of equations is rela-

TABLE II.

Reaction included in model of NO formation. Exothermicities and activation energies in Kcal and rate constants in cm^3/sec.

(1) $N + NO \Leftrightarrow N_2 + O + 75.0$;	$k_1 = 2 \times 10^{-11}$
(2) $N + O_2 \Leftrightarrow NO + O + 31.8$;	$k_2 = 2 \times 10^{-11}\ e^{-7.1/RT}$
(3) $N + OH \Leftrightarrow NO + H + 39.4$;	$k_3 = 7 \times 10^{-11}$
(4) $H + N_2O \Leftrightarrow N_2 + OH + 62.4$;	$k_4 = 5 \times 10^{-11}\ e^{-10.8/RT}$
(5) $O + N_2O \Leftrightarrow N_2 + O_2 + 79.2$;	$k_5 = 6 \times 10^{-11}\ e^{-24.0/RT}$
(6) $O + N_2O \Leftrightarrow NO + NO + 36.4$;	$k_6 = 8 \times 10^{-11}\ e^{-24.0/RT}$

tively easy, investigation has shown that the characteristic relaxation times for both N and N_2O are several orders of magnitude shorter than that for NO. It is thus an excellent approximation to assume steady state values for N and N_2O and set $dN/dt = dN_2O/dt = 0$. The set may then be reduced to a single equation for the NO formation rate:

$$\frac{1}{V}\frac{d[NO]V}{dt} = 2(1-\alpha^2)\left[\frac{R_1}{1+\alpha K_1} + \frac{R_6}{1+K_2}\right] \tag{5}$$

where $\alpha = [NO]/[NO]_e$ is the concentration of NO divided by its equilibrium value, $K_1 = R_1/(R_2 + R_3)$, $K_2 = R_6/(R_4 + R_5)$, and R_i is the « one way » equilibrium rate of the i^{th} reaction e.g. $R_1 = k_1[NO]_e[N]_e$. For the fully mixed case V is the total volume of the burned gas while for the unmixed case, which is the only one we shall consider, it is the specific volume of the burned gas. The term proportional to R_1 is the result of the first three reactions in table 2 and corresponds to the well known Zel'dovich mechanism of NO formation extended to include the reaction of N with OH. The term proportional to R_6 is the result of the last three reactions. It is this term which under some conditions is kinetically equivalent to the overall reaction $O_2 + N_2 \Leftrightarrow 2$ NO. The direct reaction $O_2 + N_2 \Leftrightarrow 2$ NO is very slow and does not contribute significantly.

TABLE III.

Ratio of rates R_1 and R_6 appearing in equation 5 for NO formation rate.

T °K	$\Phi = .8$ (lean)	1	1.2 (rich)
2500	5^{-2}	2^{-2}	3^{-3}
2300	1^{-1}	3^{-2}	4^{-3}
1800	4^{-1}	3^{-2}	6^{-4}
1500	2^{0}	4^{-2}	5^{-5}

In general K_1 and K_2 are of order unity or less and thus for $\alpha \geq 1$ the relative importance of the two terms is just determined by the ratio of R_1 to R_6. This ratio is shown in table 3 and it can be seen that for all conditions of interest it is the extended Zel'dovich mechanism which controls the NO production. Under conditions where $\alpha \gg 1$ and NO

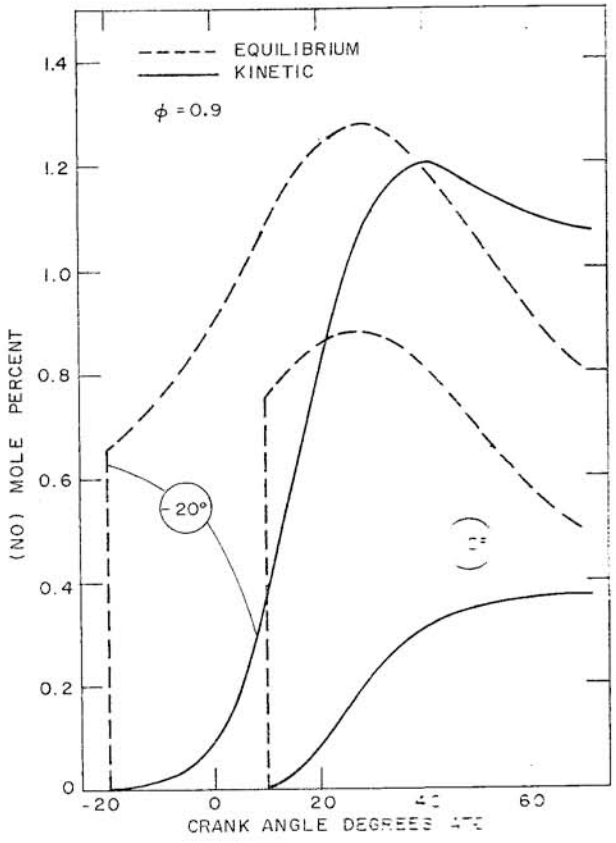

Fig. 6.

Rate controlled and equilibrium *NO* concentrations as a function of crank angle for elements which burn at two different times.

is being distroyed the second term may dominate the first, however, in this case all the reactions are very slow and the NO is effectively « frozen ».

If we now use our assumption that the concentrations of N_2, O_2, OH and O are close to equilibrium then equation [5] can easily be integrated to produce results similar to those in fig. 6. In this figure we have shown both the rate controlled and equilibrium NO concentrations as a function of crank angle for elements of gas which burned at two different times during the cycle: the first at — 20° just after ignition and the

second at + 10° when combustion was approximately 30% complete. In both cases the rate controlled solution rises from zero at a finite rate, crosses the equilibrium solution and « freezes » at levels well above the equilibrium values for exhaust temperatures. In the element of the gas which burned early the « frozen » concentrations are close to the peak equilibrium concentrations, however in the element which burned later the « frozen » levels are substantially less than the peak equilibrium

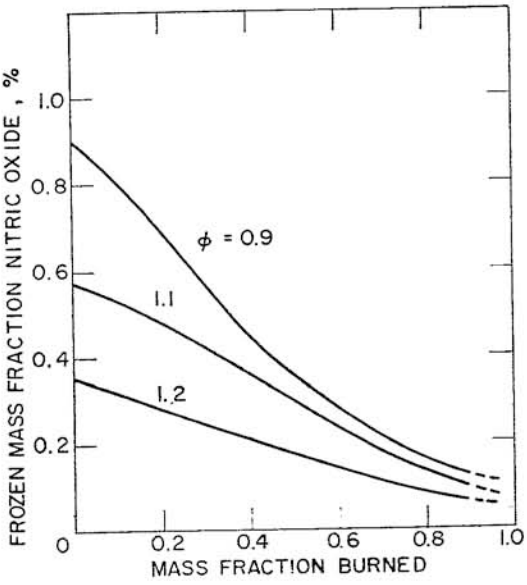

Fig. 7.

« Frozen » *NO* concentrations in the burned gas as a function of mass fraction at which an element burned for several equivalence rations.

value. This is a direct result of the very much slower reaction rates associated with the lower temperature of the gas which burns later in the cycle.

Additional results illustrating the strong effect of the temperature gradient in the burned gas on NO formation are presented in fig. 7 which shows the « frozen » mass fraction of NO in an element of gas as a function of the mass fraction at which it burned for several equivalence ratios. It can be seen that the NO concentrations in the first part of the gas to burn are 5 to 10 times those in the last part.

Observations of NO Formation.

To check on the validity of the theoretical model just described, a variety of experimental studies of NO formation in internal combustion engines are being performed. In the first such experiment [3] the NO con-

centration in the cylinder of an actual engine was measured as a function of time and position. A schematic of the L-head engine employed is shown in fig. 8. The head was fitted with a number of quartz windows W which permitted observation of a relatively uniform sample of gas at various distances from the spark. Both spectrocopic and photometric measurements were made.

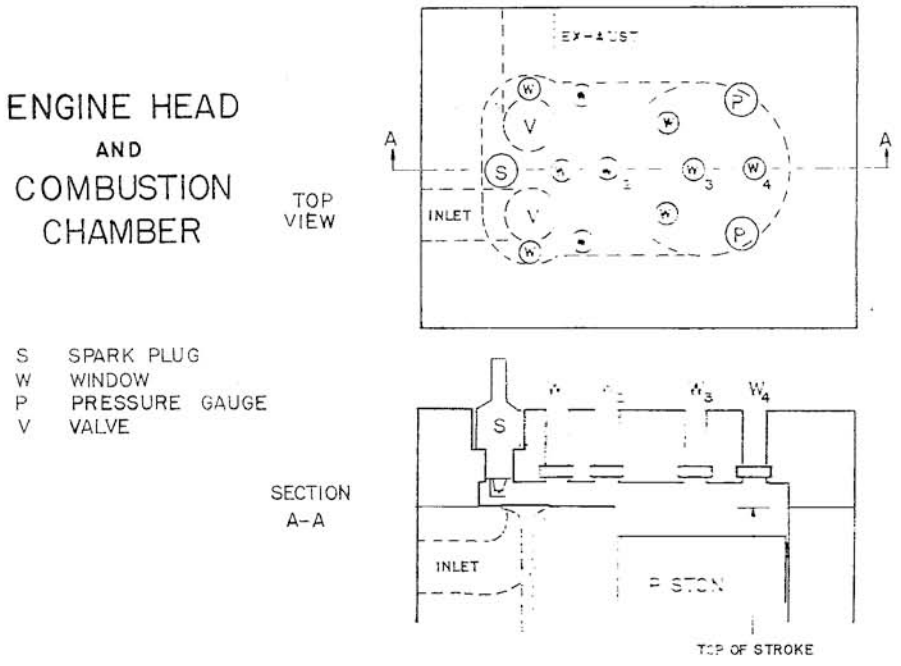

Fig. 8.

Schematic of engine head used in experiments to measure NO formation rate.

The spectral distribution of the major radiation is shown in fig. 9. In the blue it consists primarily of molecular bands of OH and a recombination continuum from the reaction $CO - O \rightarrow CO_2 + h\nu$. In the red it consists of unresolved bands of NO_2 superimposed on a continuum from the reaction $NO + O \rightarrow NO_2 + h\nu$. A few discrete lines from Na and K and weak molecular bands from CH, C_2 and H_2O were also observed.

Quantitative measurements of the radiation intensity were made using photomultipliers and narrow band interference filters. Typical oscillograms of the radiation profiles at several wavelengths are shown in fig. 10 for two cases: one in which the engine was operating on a normal fuel-air mixture and another which was identical in all respects except for the addition of 1.5% NO to the charge. Also shown are pressure traces and timing traces with markers at 5° intervals.

For the normal mixture the radiation profiles show a relatively narrow rather irregular peak, corresponding to nonequilibrium radiation from the turbulent flame front, followed by a larger broader peak corresponding to radiation from the burned gas. Note that at wavelengths of 0.61 and 0.68, where the radiation is due to NO and NO_2, the intensity

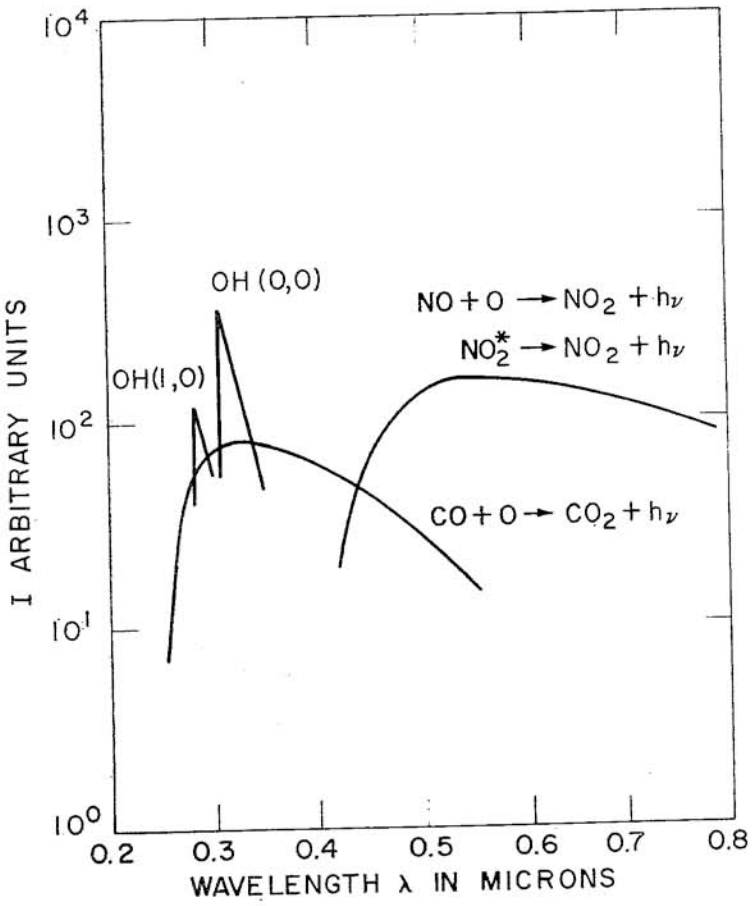

Fig. 9.

Spectral distribution of major radiation emitted by burned gas in an internal combustion engine.

immediately behind the flame front is very small indicating negligible NO formation in the flame front. By contrast when 1.5%NO is added to the charge the radiation at these wavelengths jumps abruptly to the value expected for this amount of NO at the burned gas temperature. The radiation at 0.38 microns is unaffected, however, since NO does not radiate at this wavelength and the small amount added has a negligible influence on the thermodynamic state of the burned gas. Although the

NO concentrations can be calculated from the observed radiation using known rate constants, the NO addition technique provided a direct calibration of the system and greatly increased our confidence in the results.

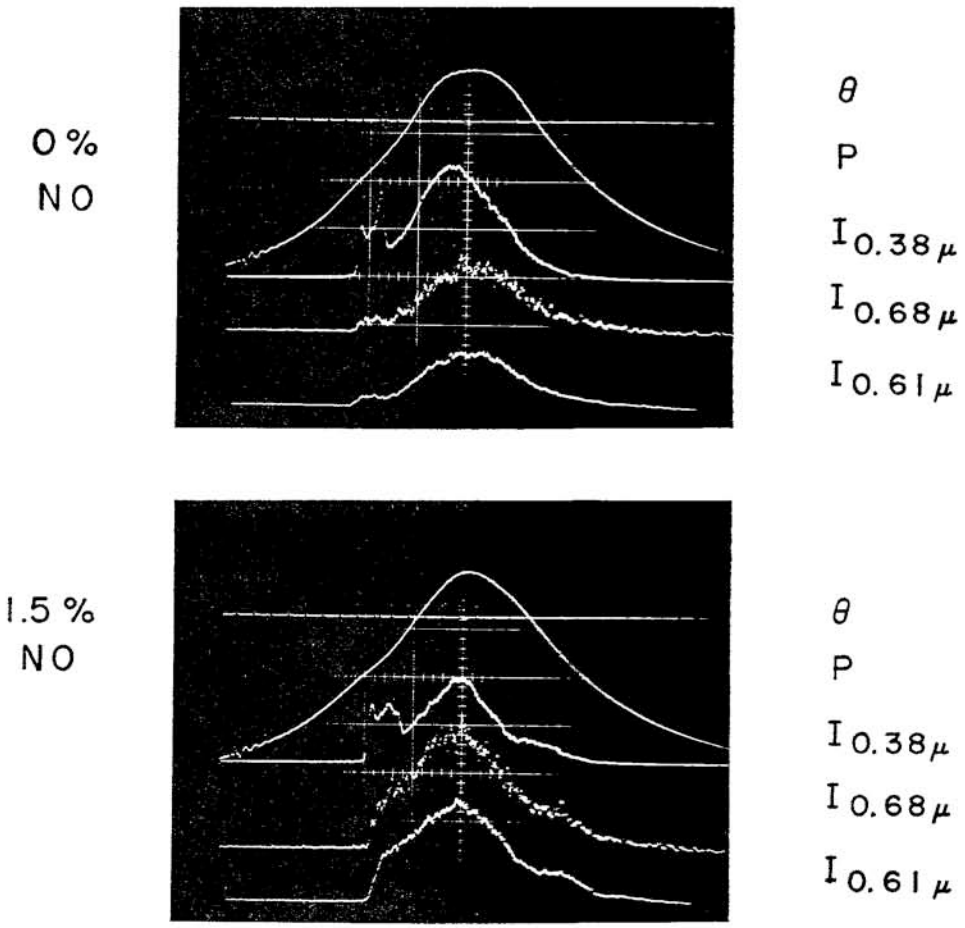

Fig. 10.

Oscillograms showing crank angle (5° markers), pressure, and radiation intensity at several wave lengths as a function of time. Upper traces correspond to a normal fuel-air mixture; lower traces to the same fuel-air mixture with NO added.

Independent measurements of the temperature of the burned gas were obtained by analyzing the radiation from the OH bands and the CO_2 continuum [6]. These agreed with each other and with that calculated from the thermodynamic model to $\pm$ 100° K.

Fig. 11 shows the measured NO concentrations as a function of crank angle for two equivalence ratios [6]. The open symbols correspond

to normal fuel-air mixtures and the closed symbols to mixtures with 1.5% NO added. The stars indicate the NO levels at the flame front. In the case of the normal mixture this is the estimated level due to the residual burned gas in the cylinder. For the normal mixtures, the NO concentrations rise monotonically approaching a constant « frozen » level. For the mixtures with NO added, the concentrations first decrease since they

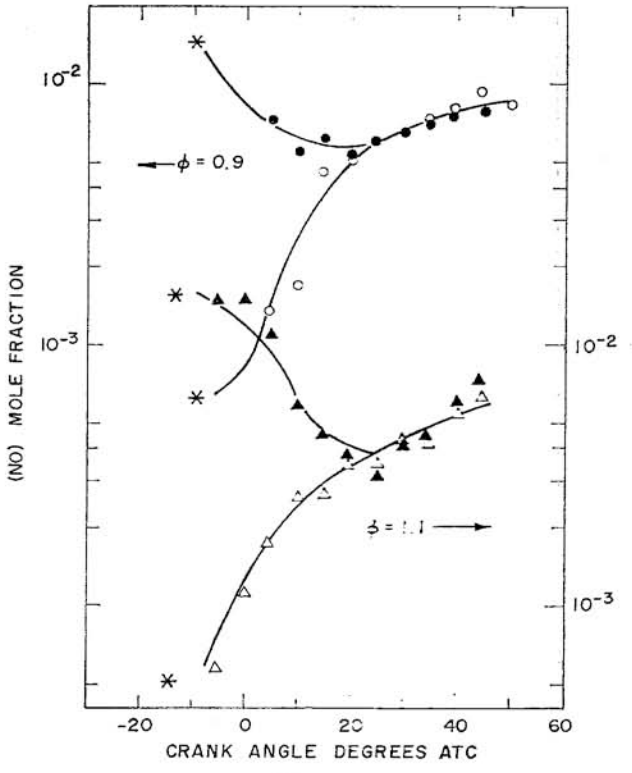

Fig. 11.

NO concentrations as a function of crank angle for two equivalence ratios with and without 1.5% added *NO*.

are above the equilibrium value, then go through minima and join the curves for the normal mixtures exactly as we would predict.

A comparison between theoretical and experimental results is presented in fig. 12 which shows the measured [6] and predicted NO concentrations at two distances from the spark as a function of crank angle. Unfortunately the theoretical curves were started from zero because the presence of NO in the residual gas was overlooked at the time they were computed. Even so the agreement between theory and experiment is very satisfactory. Note the higher level of NO at window W_2, which was

closer to the spark, due to the higher temperature in the gas that burns first.

Fig. 13 shows a further comparison between theory and experiment. Here the average levels of NO in the exhaust are plotted as a function of equivalence ratio. For equivalence ratios less than 1.2 the measured [7]

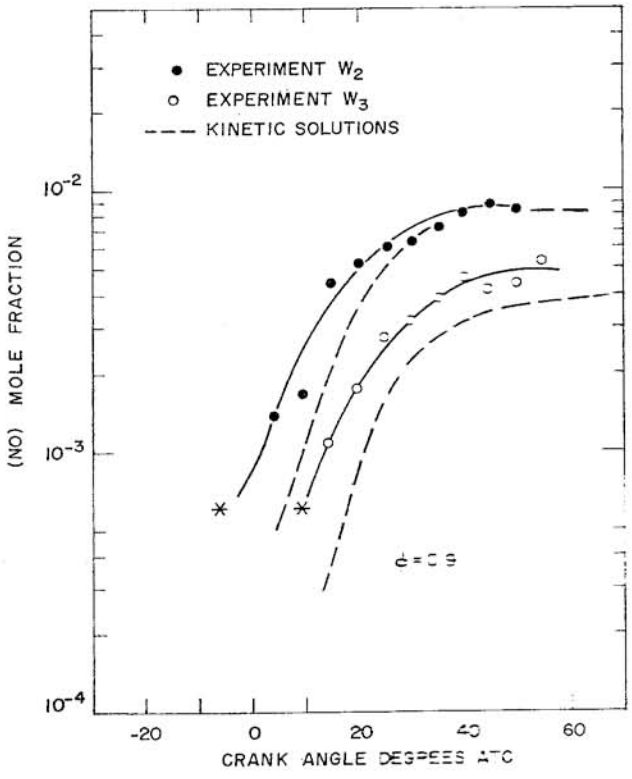

Fig. 12.

Comparison between predicted and measured *NO* concentrations at two distances from the spark as a function of crank angle. The theoretical curves neglect the *NO* initially present due to the residual gas and are therefore expected to be low at early times.

and predicted values are in good agreement. For richer mixtures, however, the theory appears to underestimate the NO concentrations somewhat. This may be the result of NO formation in the flame front or a parallel reaction not included in the kinetic scheme.

It is fairly clear from the results presented above that most of the NO production in internal combustion engines occurs in the burned gas and that the important parameters controlling the levels are the gas temperature and the equivalence ratio. Fuel composition is expected to have very little effect. Thus to reduce NO emission one most run either

rich or reduce the peak temperatures. The latter may be accomplished in a variety of ways including: lean combustion, retarded spark, lower compression ratio, central spark, and exhaust gas recirculation or water injection.

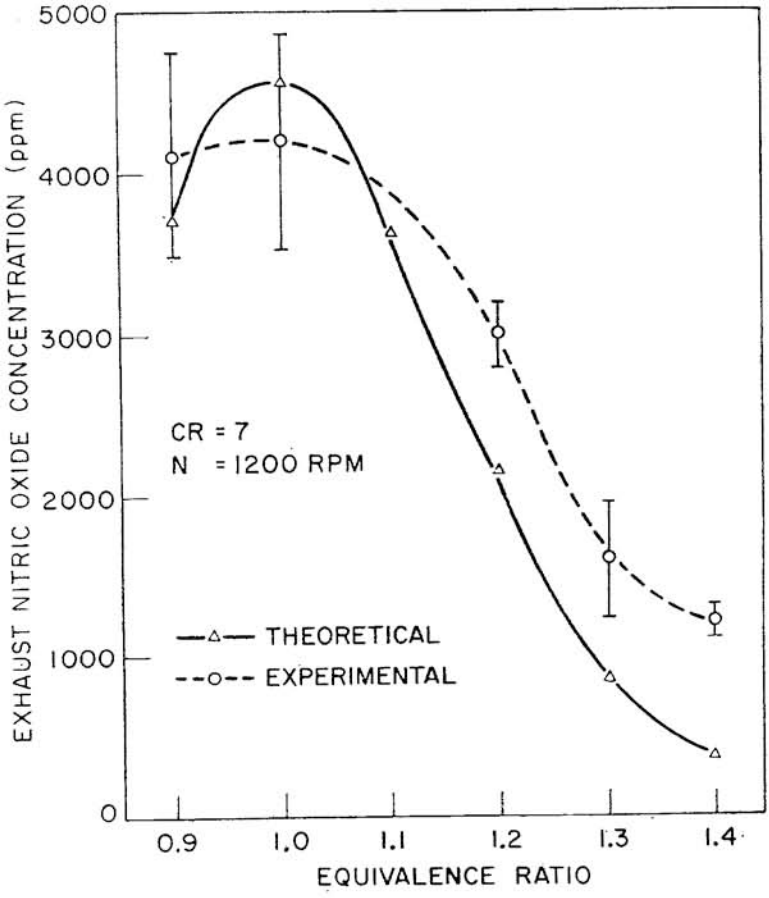

Fig. 13.

Comparison between predicted and measured average NO concentrations in the exhaust as a function of equivalence ratio.

Mechanism of CO « Freezing ».

In our previous analysis we have assumed that the major energy producing reactions involving the C—O—H system were in thermodynamic equilibrium near peak cylinder temperatures. If this were true at exhaust temperatures then the CO levels would be completely negligible. We must therefore consider departure from equilibrium in the C—O—H

system as the temperature falls during expansion. This is a formidable problem which is extremely difficult to treat using the ordinary techniques for solving rate equations in complex systems. To deal with it we have developed a new approach which we have called the « rate-controlled partial-equilibrium method ». It is based on the observation that the existence of a slow chemical reaction in a system implies a constraint on the rate at which the system can adjust to full equilibrium. Examples of such constraints are provided by nuclear reactions which proceed extremely slowly at ordinary temperatures and imply conservation of atomic species.

The first step in the method is to identify the constraints which would exist if a particular reaction or set of reactions did not proceed at all. Such constraints are usually of the form

$$N_i = \sum_j a_{ij} X_j \tag{6}$$

where X_j is the number of molecules of species j, a_{ij} is an integer greater than or equal to zero, and N_i is the constrained variable. We next consider the Gibbs free energy of the system

$$F(T, p) = \sum_j X_j[F_j + RT \ln (X_j/X_0)] \tag{7}$$

where F_j is the free energy of species j and $X_0 = \sum_j X_j$. The partial equilibrium state may now be found by minimizing $F(T, p)$ subject to the constraints N_i in the usual manner. Finally the rate at which the constraint changes is determined from the chemical reaction rates. This leads to equations of the form

$$\frac{d N_i}{dt} = R_i(X_1, X_2, \ldots X_n) \tag{8}$$

which may be integrated numerically to obtain the partial equilibrium composition as a function of time.

The advantage of this method over the commonly used steady state approximation or integration of the full set of rate equations is that only the rate limiting reactions need to be specified. This reduces the number of equations to be integrated by a large factor and avoids the problem that most of the chemical reaction rates in a complex system are unknown and must therefore be guessed.

As an initial application of the method we have used it to investigate the effect of finite three-body recombination and dissociation rates.

The constraint introduced by inhibiting such reactions is of the form $M = \sum_j X_j$ where M is the total number of particles in the system. The rate equation for M is of the form

$$\frac{dM}{dt} = \sum_k (R_{dk} - R_{rk}) \tag{9}$$

where R_{dk} and R_{rk} are the dissociation and recombination rates for the k^{th} reaction. Some three-body reactions important in internal combustion engines are shown in table 4. In our present analysis we have included only the first three. In this connection it should be noted that only one fast three-body reaction is needed to equilibrate the entire system, however, different reactions will dominate in different temperature ranges. At peak temperatures it will be first, at intermediate temperatures where NO is frozen it is expected to be the second, and at room temperature it will be the third.

TABLE IV.

Examples of threebody recombination and dissociation reactions of potential importance in internal combustion engines. Exothermicities and activation energies in Kcal and recombination rate constants in cm⁶/sec.

$118.0 + H_2O + X \Leftrightarrow OH + H + X$	:	3×10^{-31}
$71.9 + NO_2 + X \Leftrightarrow NO + O + X$	:	6×10^{-32}
$25.8 + NO_2 + NO_2 \Leftrightarrow NO + NO + O_2$	:	1×10^{-38}
$38.6 + {}^1N_2O + X \Leftrightarrow {}^1N_2 + {}^3O + X$		
$125.8 + {}^1CO_2 + X \Leftrightarrow {}^1CO + {}^3O + X$	:	1×10^{-34}
$21.4 + HCO + X \Leftrightarrow CO + H + X$		

Some typical results for a stoichiometrically correct high temperature cycle are presented in fig. 14 as a function of crank angle and equilibrium temperature. The upper part of the figure shows the mole fraction of CO, NO, O and N. The subscripts e and M denote the equilibrium and three-body rate controlled solution respectively. On the scale of the figure the difference between the two solutions is indistinguishable. The central part of the figure shows the difference between the rate controlled and equilibrium CO mole fractions and it can be seen that this is very small. Finally the lower part of the figure shows the difference between the rate controlled and equilibrium temperatures which is also very small. These results support our previous assumption that the burned gas is close to thermodynamic equilibrium at peak temperatures.

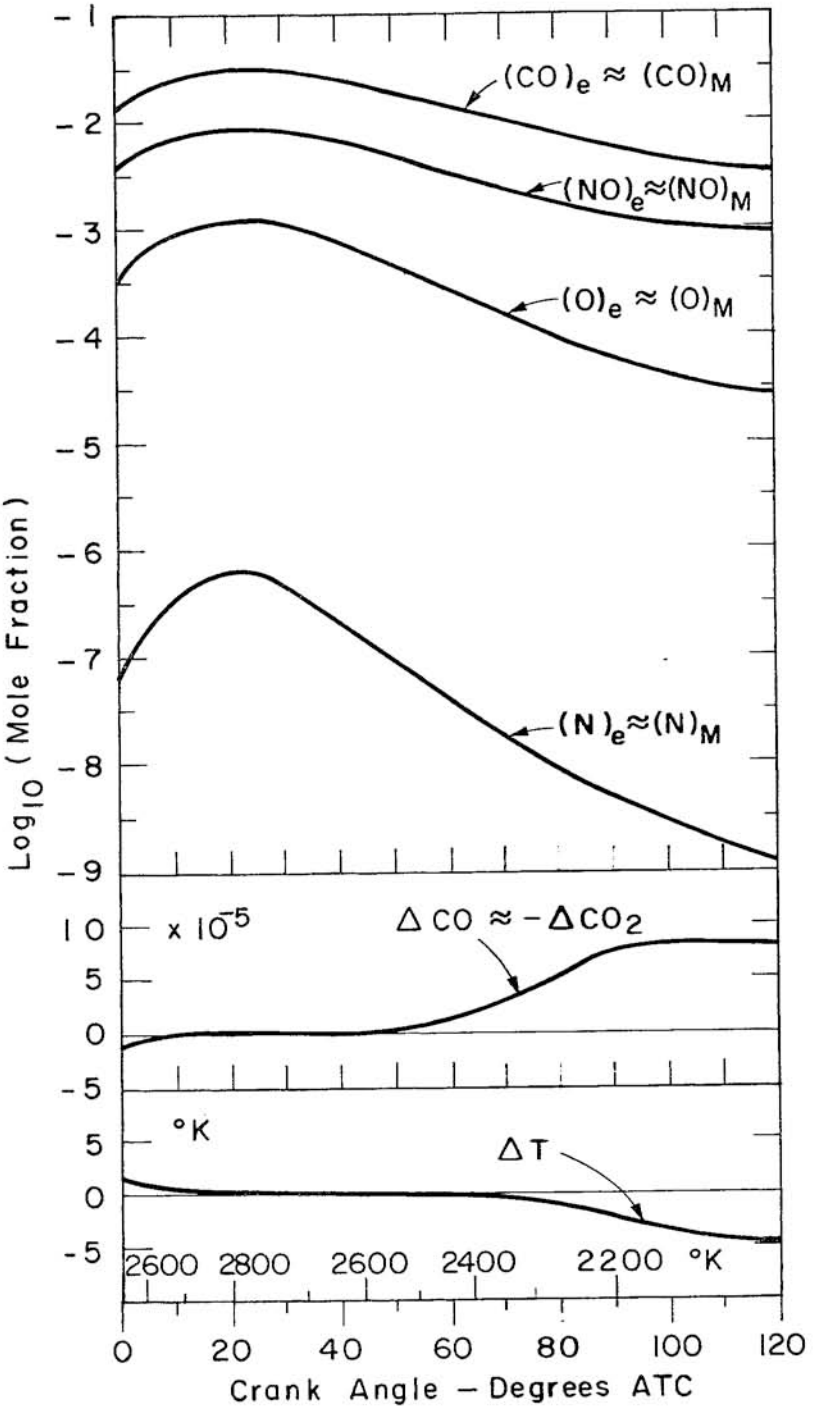

Fig. 14.

Comparison of rate controlled (subscript *M*) and equilibrium (subscript *e*) concentration and temperatures as a function of crank angle and equilibrium temperature for a cycle with a peak temperature of 2800 °K.

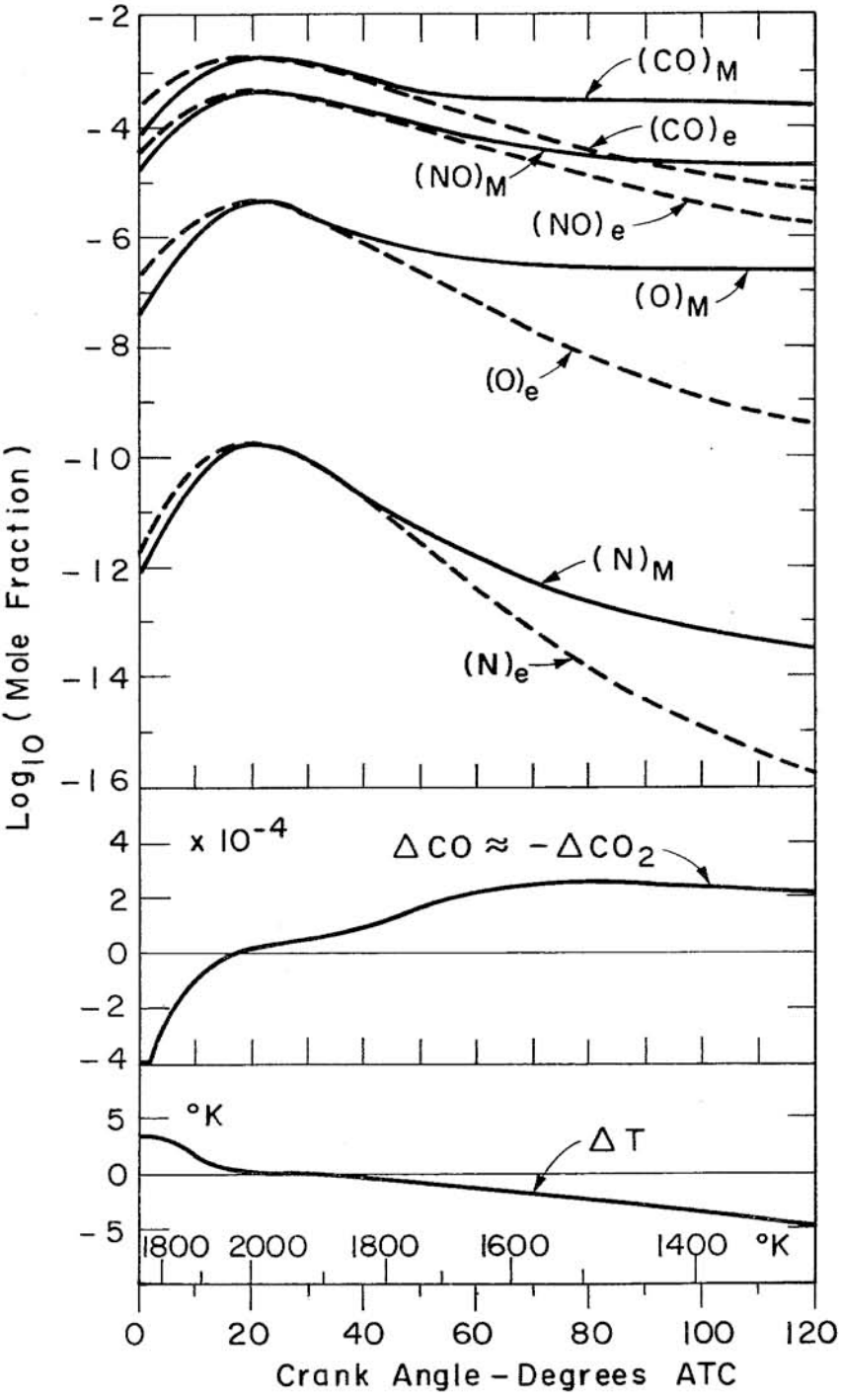

Fig. 15.

Comparison similar to that of figure 14 for a cycle with a peak temperature of 2000 °K.

By way of contrast similar results for a very low temperature cycle are shown in fig. 15. In this case significant differences between the rate controlled and equilibrium solutions occur for all species. At early times the rate controlled concentrations lag behind the equilibrium concentrations because of the finite dissociation rates. Full equilibrium is achieved near the peak temperature and maintained for a short time as the temperature falls to approximately 1800° K where « sudden freezing » of the threebody reactions occurs. Beyond this point changes in the rate controlled concentrations particularly of CO and NO become negligible. Note that the « frozen » CO mole fraction of approximately 0.1% is very close to the values actually observed in the exhaust of well adjusted internal combustion engines. Also note that the « freezing » of NO in this case is associated with finite threebody recombination rates and not with the reactions in table 2 which were tacitly assumed to be in equilibrium in the partial equilibrium solution.

The partial equilibrium method is currently being extended to include simultaneous consideration of finite rates for both NO producing and recombination-dissociation reactions. It is hoped that this extension will permit us to develop a model for predicting CO as well as NO emissions. It is also hoped that it may help to explain why our current model of NO production underestimates the concentrations in rich mixtures.

Concluding Remarks.

On the basis of the work we have performed to date, we believe that it should be possible to understand a great deal about the fundamental mechanism of pollutant formation in internal combustion engines and to develop quantitative models of the important processes which will be of practical value in designing low pollution engines and assessing their relative merits. I have no doubt that reduction of pollution from internal combustion engines to acceptable levels is technically feasible using a variety of methods. The problem is to find the best combination and to convince government and industry that it is worth the effort and cost.

REFERENCES

[1] W. A. DANIEL and J. T. WENTWORTH, Paper 486 B presented at S. A. E. National Automobile Week, March 1962.

[2] R. J. TABACZYNSKI, D. P. HOULT, and J. C. KECK, *Fluid Mech.*, 42, 249 (1970).

[3] G. A. LAVOIE, J. B. HEYWOOD, and J. C. KECK, *Combustion Science and Technology*, 1, 313 (1970).

[4] H. K. NEWHALL and E. S. STARKMAN, Paper 670122 presented at S. A. E. Automotive Engineering Congress 1967; P. EYZAT and J. C. GUIBET, Paper 680124 presented at S. A. E. Automotive Engineering Congress 1968.

[5] K. SCHOFIELD, *Planet. Space Sci.*, 15, 643 (1967); I. M. CAMPBELL and B. A. THRUSH, « *Trans. Faraday Soc.*, 64, 1265 (1968).

[6] G. LAVOIE, *Combustion and Flame*, 15, 97 (1970).

[7] J. B. Heywood, S. M. MATHEWS, and B. OWEN, Paper 710011 presented at S. A. E. Automotive Engineering Congress, January 1971.

ESTRATTO DAGLI *Atti del Convegno su*

« Problemi attuali connessi con lo sviluppo tecnologico ed economico del Piemonte e regioni limitrofe »

Accademia delle Scienze di Torino
(Torino, 27-28 settembre 1970)